PCCP

PAPER

Cite this: *Phys. Chem. Chem. Phys.*, 2016, **18**, 21391

A comparative first-principles study of the lithiation, sodiation, and magnesiation of black phosphorus for Li-, Na-, and Mg-ion batteries†

K. P. S. S. Hembram, Hyun Jung, Byung Chul Yeo, Sung Jin Pai, Heon Ju Lee, Kwang-Ryeol Lee and Sang Soo Han*

Received 29th March 2016,
Accepted 11th July 2016

DOI: 10.1039/c6cp02049f

www.rsc.org/pccp

Using first-principles calculations, we describe and compare atomistic lithiation, sodiation, and magnesiation processes in black phosphorous with a layered structure similar to graphite for Li-, Na-, and Mg-ion batteries because graphite is not considered to be an electrode material for Na- and Mg-ion batteries. The three processes are similar in that an intercalation mechanism occurs at low Li/Na/Mg concentrations, and then further insertion of Li/Na/Mg leads to a change from the intercalation mechanism to an alloying process. Li and Mg show a columnar intercalation mechanism and prefer to locate in different phosphorene layers, while Na shows a planar intercalation mechanism and preferentially localizes in the same layer. In addition, we compare the mechanical properties of black phosphorous during lithiation, sodiation, and magnesiation. Interestingly, lithiation and sodiation at high concentrations (Li_2P and Na_2P) lead to the softening of black phosphorous, whereas magnesiation shows a hardening phenomenon. In addition, the diffusion of Li/Na/Mg in black phosphorus during the intercalation process is an easy process along one-dimensional channels in black phosphorus with marginal energy barriers. The diffusion of Li has a lower energy barrier in black phosphorus than in graphite.

1. Introduction

The growing interest in energy storage systems (ESSs) has led to the search for next-generation batteries beyond Li-ion batteries (LIBs) because the geographic maldistribution of Li reserves may cause a rapid increase in the price of Li as the demand for LIBs grows exponentially.[1,2] Beyond LIBs, Na-ion batteries (NIBs) and Mg-ion batteries (MIBs) have received considerable attention and the development of relevant electrode materials has become an important scientific issue.

Graphite has been regarded as the standard anode material in LIBs because it forms stable Li-intercalated graphite forms such as LiC_6 and it has a rapid charge/discharge rate due to its two-dimensional layered structure.[3,4] However, Na and Mg have been difficult to intercalate into graphite, most likely because of the large ionic radius of Na (0.95 Å for Na^+ > 0.65 Å for Mg^{2+} > 0.60 Å for Li^+) and the high ionization potential of Mg (7.65 eV for Mg > 5.39 eV for Li > 5.14 eV for Na).[5] This behavior indicates that graphite is unsuitable for NIBs and MIBs.

Recently, many researchers have become interested in black phosphorus, which is the most stable of the three phosphorus allotropes (red, white, and black),[6,7] because it has a layered structure similar to graphite but a different electronic structure (semi-metallic for graphite *versus* semiconducting for black phosphorus). The interlayer distance of black phosphorus is greater than that of graphite (5.4 Å for black phosphorous *vs.* 3.4 Å for graphite),[7,8] implying easier intercalation of ions between its layers. The environmental friendliness and abundance of phosphorus are other important features that make it an economical material. For these reasons, black phosphorus materials have been recently studied for use in promising electronic and energy storage materials. Indeed, several experiments have shown that black phosphorus could be a good platform for LIBs, where commonly used electrolytes such as ethylene carbonate have been used.[9–17] Other experiments have reported that black phosphorus can be used as an anode for NIB applications.[18–21] However, to the best of our knowledge, there have been no studies exploring the possibility of the use of black phosphorus in MIBs.

To improve the performance of LIBs, NIBs, and MIBs that use black phosphorus, understanding the lithiation, sodiation, and magnesiation processes in black phosphorus at the atomic

Computational Science Research Center, Korea Institute of Science and Technology (KIST), Hwarangno 14-gil 5, Seongbuk-gu, Seoul, 136-791, Republic of Korea. E-mail: sangsoo@kist.re.kr; Fax: +82 2958 5451; Tel: +82 2 958 5441

† Electronic supplementary information (ESI) available: Radial distribution function and formation of tunnel-like channels in black phosphorus during lithiation, sodiation, and magnesiation, and equation of states of M_2P (M = Li, Na, and Mg). See DOI: 10.1039/c6cp02049f

scale is very important. Recently, we have successfully explored a systematic sodiation mechanism of black phosphorus using first-principles calculations;[22] however, the corresponding lithiation and magnesiation processes have not yet been reported. In this work, using first-principles calculations, we first report a comparative work on the atomistic lithiation, sodiation, and magnesiation mechanisms and compare their electronic and mechanical properties along with their kinetic properties. We thereby conclude that black phosphorus could be a promising platform material for LIBs, NIBs, and MIBs.

In addition, the solid–electrolyte interface (SEI) is one of the critical factors to determine battery performance such as cyclic properties and safety. The relevant research is definitely important. However, in this work, we focus on unraveling the atomistic lithiation, sodiation, and magnesiation mechanisms of black phosphorus, which have not clearly been reported yet. Thus, the SEI study on the black phosphorus anode remains as our future work.

2. Computational methods

We performed periodic *ab initio* density functional theory (DFT) calculations as implemented in the Vienna *ab initio* simulation package (VASP).[23,24] The exchange–correlation energy is described by the generalized gradient approximation (GGA) proposed by Perdew, Burke and Ernzerhof (PBE).[25] The electronic wave functions were expanded using a plane wave basis set with a kinetic energy cutoff of 500 eV. The effects of core electrons were replaced by projector augmented wave (PAW) potentials.[26] To include the effects of van der Waals interactions, we adopted Grimme's DFT-D2 approach[27] implemented in VASP.

To investigate the insertion mechanisms and diffusion behaviors of Li, Na, and Mg atoms in black phosphorus, we considered a black phosphorus model using a 2 × 2 × 2 supercell with four phosphorene layers (total of 64P atoms). The Brillouin zone was sampled using a 3 × 2 × 1 Monkhorst–Pack grid.[28] The atomic structures of M_xP were fully optimized without any symmetry constraint. For structural optimizations, the magnitudes of the forces on the atoms were minimized to below the limit of 10^{-3} eV Å^{-1}. Our calculation provides the lattice parameters of the black phosphorus crystal (a = 3.32 Å, b = 4.41 Å, and c = 10.49 Å), which are similar to the experimental and theoretical values (a = 3.34 Å, b = 4.49 Å, and c = 10.81 Å).[29,30]

In finding optimized structures of M_xP with layered structures, we considered all of the possible cases of intercalation. On the other hand, for amorphous M_xP structures, the M guest atoms were initially placed randomly in the crystalline black phosphorus by using a random number generator algorithm. The structures were optimized by *ab initio* molecular dynamics (AIMD) simulation at 300 K, and then the AIMD structures were further relaxed using a conjugate-gradient method. We expect that the structures obtained from this procedure could provide the minimum energy configurations.

3. Results and discussion

3.1. Lithiation, sodiation and magnesiation mechanisms

To unravel the lithiation, sodiation, and magnesiation processes of black phosphorus, we calculated the M_xP formation energies as functions of the M concentrations (M = Li, Na and Mg) using the following equation:

$$E_f(x) = E_{tot}(M_xP) - E_{tot}(P) - xE_{tot}(M) \quad (1)$$

where $E_{tot}(M_xP)$ is the total energy per M_xP unit, $E_{tot}(P)$ is the total energy per atom in the bulk black phosphorus, $E_{tot}(M)$ is the total energy per atom in the bcc M crystal (for Li and Na) or hcp M crystal (for Mg), and x is the concentration of M atoms. For a given x of M_xP, we considered various configurations, optimized the systems with full structural relaxation, and selected the optimized structures to clarify the insertion mechanisms.

Fig. 1 shows the calculated formation energies and volume expansions of the M_xP systems. The stabilities of the systems are in the order Li_xP > Na_xP > Mg_xP, whereas the volume expansions are in the order Na_xP > Mg_xP > Li_xP. The volume expansion order is attributed to the ionic radii of the metals: Na^+ (0.95 Å) > Mg^{2+} (0.65 Å) > Li^+ (0.60 Å). According to the calculated formation energies, black phosphorus can store alkali-metal atoms at concentrations up to $Li_{4.5}P$, $Na_{4.0}P$, and $Mg_{2.0}P$.

Based on the calculated formation energies of various M_xP systems, the atomistic lithiation, sodiation, and magnesiation mechanisms of black phosphorus are shown in Fig. 2. We first investigated whether two M atoms that intercalated into the black phosphorus preferred being in the same layer or in different layers in the formation of M_2P_{64} ($M_{0.03}P$) systems. Two Li/Mg atoms prefer to occupy adjacent layers in black phosphorus (columnar intercalation); in contrast, two Na atoms prefer to stay in the same layer (planar intercalation). This intercalation behavior is determined by the atomic charges of the M atoms and the increased interlayer spacing after intercalation. According to Bader charge analysis, the atomic charges of Li, Na, and Mg in $M_{0.03}P$ are +0.84e, +0.78e, and +1.51e, respectively, and they exert repulsive forces between one another. Considering only the atomic charge, Li, Na, and Mg should all prefer to be in different layers. However, the intercalation of the Li/Na/Mg atoms into the same layer space leads to a smaller increase of the interlayer space than in different layers and hence the lower energy cost. By comparing with

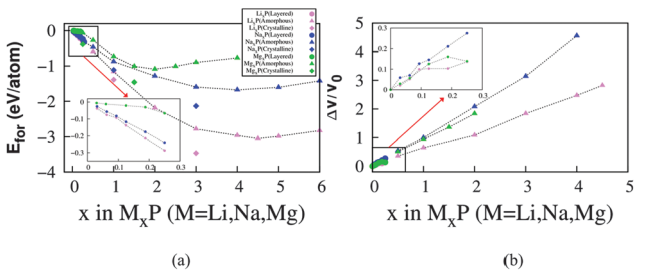

Fig. 1 (a) Calculated formation energy and (b) volume expansion of M_xP systems (M = Li, Na and Mg). Here, the inset in each figure corresponds to data for the layered black phosphorous region at low M concentrations.

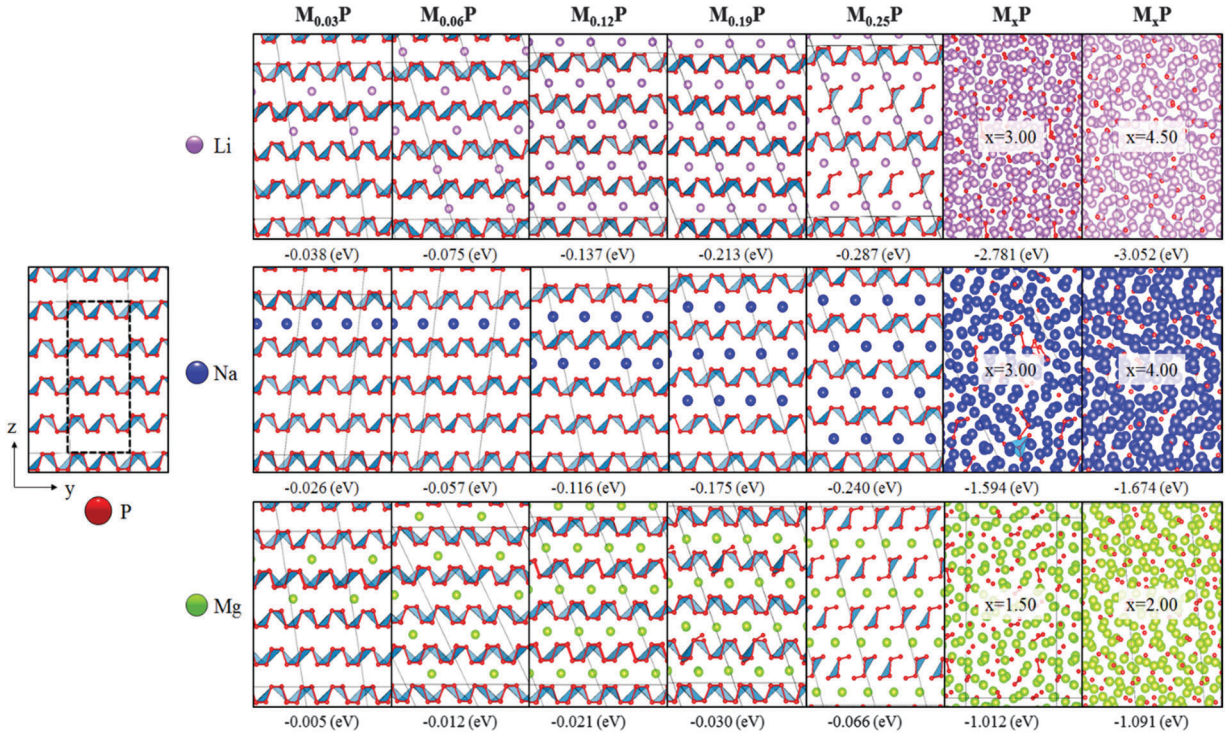

Fig. 2 Insertion mechanism in black phosphorus with an increase in concentration of Li, Na and Mg. The solid gray line represents a supercell containing 64 P atoms, and the number represents the formation energy.

Li and Mg atoms in $M_{0.03}P$, Na atoms have a lower atomic charge, which indicates that Na atoms in the same layer space exert less repulsive forces between one another than Li and Mg cases. In the case of Na, the energy compensation induced by occupying the same layer is higher than the energy loss induced by the Coulomb repulsion between Na atoms, which is in contrast to Li and Mg cases. Because of these reasons, two Na atoms occupy the same layer, although Li and Mg atoms prefer to occupy the different layers. Here, one needs to remember that the volume expansion of $Na_{0.03}P$ is larger than that of $Li_{0.03}P$ due to the larger ionic radius of Na^+, as shown in Fig. 1.

When two more Li/Na/Mg atoms are added into the $M_{0.03}P$ structures, similar behaviors are still found. In other words, the Li/Mg atoms prefer to occupy different layers, while the Na atoms prefer to occupy the same layer. This intercalation process proceeds up to θ = 25% coverage per phosphorene layer; however, there is no P–P bond breaking in $Na_{0.25}P$, while in both $Li_{0.25}P$ and $Mg_{0.25}P$, the breaking of some P–P bonds is observed together with no P–P bond breaking in $Li_{0.19}P$ and $Mg_{0.19}P$. At the critical point ($Li_{0.19}P$, $Mg_{0.19}P$, and $Na_{0.25}P$), the insertion mechanism for all three metals changes from an intercalation process to an alloying process.

Black phosphorus has a corrugated structure, with two different P–P bond types: *planar* P–P and *staggered* P–P. Below the critical points for the changes in the insertion mechanisms of Li, Na, and Mg, the chemical bonds between P atoms in black phosphorus are not significantly affected, and there is no P–P bond dissociation, although the interlayer distance increases. In other words, at the critical points of lithiation ($Li_{0.19}P$), magnesiation ($Mg_{0.19}P$), and sodiation ($Na_{0.25}P$), all of the planar P–P distances are 2.2 Å, and all of the staggered P–P distances are 2.3 Å, similar to those of pristine black phosphorus (2.2 Å for planar and 2.3 Å for staggered). However, the interlayer distances of $Li_{0.19}P$ (6.2 Å), $Mg_{0.19}P$ (6.5 Å), and $Na_{0.25}P$ (6.8 Å) are longer than the 5.4 Å distance of the pristine material.

During the alloying processes, which occur above the critical concentrations ($Li_{0.19}P$, $Mg_{0.19}P$, and $Na_{0.25}P$), P–P bonds start to break, and then, low-coordinated P clusters, such as dumbbells, are generated. According to the radial distribution function (RDF) analysis in the ESI† (Fig. S1), the P–P distances increased with the Li/Na/Mg concentration, which induces the amorphization of black phosphorus, although it is similar up to a concentration of $M_{0.25}P$ (M = Li, Na, and Mg). On the other hand, the Li–Li, Na–Na, and Mg–Mg peaks shift to shorter distances with increasing Li/Na/Mg concentration. A similar trend is also observed in the lithiation of Si and sodiation of Si, Ge, and Sn systems.[31,32]

During the early stages of the intercalation of guest M metal atoms into host black phosphorus, one guest atom tends to bind to the P atoms in black phosphorus, which induces the sliding of phosphorene layers followed by structural distortion. In other words, the sliding of adjacent layers creates a tunnel-like structure (Fig. S2, ESI†), which occurs due to the slipping motion between two adjacent phosphorene layers. This phenomenon is also observed in other theoretical reports.[22,33] The sliding has a low energy cost (0.08 eV per atom), suggesting that the sliding of the phosphorene layers is easy.[22] During lithiation and magnesiation, which prefer interlayer intercalation, the sliding of layers is almost complete in the early intercalation stage at $(Li/Mg)_{0.06}P$.

On the other hand, in the case of sodiation, this process occurs stepwise up to $Na_{0.25}P$. The relative sliding of layers also leads to a change in the shape of the structure (*i.e.*, the original tetragonal shape of black phosphorus changes to a trapezoidal structure).

As already mentioned, the alloying process involving P–P bond breaking starts at the critical point of $Li_{0.19}P$, $Mg_{0.19}P$, and $Na_{0.25}P$. The P–P bond breaking behavior would not be beneficial for the cyclic properties of the black phosphorus anode. As one option to improve the properties, a black phosphorus–graphite composite can be considered, where the formation of stable phosphorus–carbon bonds would enhance the stability of the layered structure of black phosphorus. Indeed, this is supported by a recent experiment.[17]

3.2. Comparison of the M_xP electronic structures (M = Li, Na, and Mg)

The difference in the intercalation mechanisms of Li/Mg and Na atoms in black phosphorus can be confirmed through electronic structure analysis. Fig. 3 shows the partial densities of states (PDOSs) of electrons in $M_{0.06}P$ (M = Li, Na, and Mg) systems. At the Fermi level, the contributions of the Li 2s and Mg 3s orbitals are comparable to that of the P 3p orbital, while the contribution of the Na 3s orbital is very low compared with that of the P 3p orbital. This behavior results from the difference in the intercalation mechanisms of Li/Mg (columnar intercalation) and Na (planar intercalation) in black phosphorus. Li/Mg atoms preferentially tend to localize in different phosphorene layers in black phosphorus, where the metal atoms show greater interaction with the P atoms than when they are located in the same phosphorene layer, as found in the Na case. Thus, more s orbitals of Li and Mg contribute at the Fermi level.

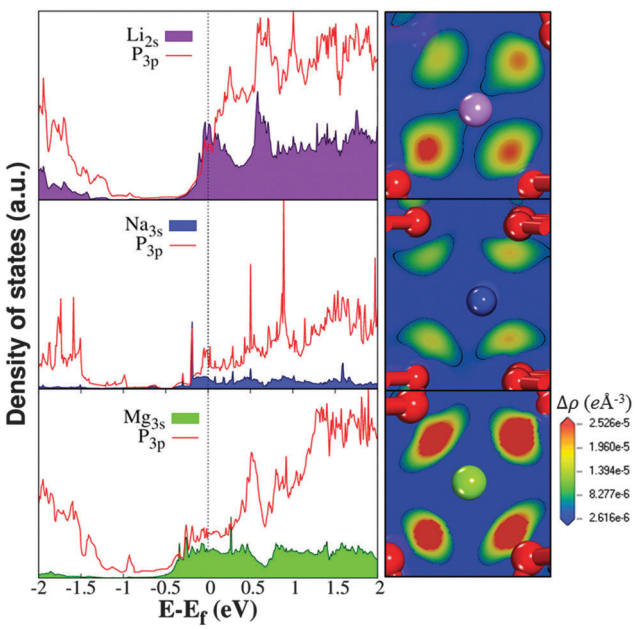

Fig. 3 Partial electron densities of states (right) and valence electron charge density differences (left) in $M_{0.06}P$ (M = Li, Na, and Mg). Here, pink, blue, green, and red atoms are Li, Na, Mg, and P atoms, respectively.

We additionally calculated the charge density differences in $M_{0.06}P$ (M = Li, Na, and Mg) to investigate the bonding character between M and P atoms, which is also plotted in Fig. 3 along with the PDOS data. The charge density difference $\Delta\rho$ is defined as

$$\Delta\rho = \rho_{M_{0.06}P} - \rho_P - \rho_M \quad (2)$$

where $\rho_{M_{0.06}P}$, ρ_P, and ρ_M are the electron densities of the $M_{0.06}P$ system, a phosphorus structure consisting of only P atoms in the same positions as in the $M_{0.06}P$ structure, and the contribution from the individual M atoms at the positions they occupy in the $M_{0.06}P$ system, respectively. The Li–P bonds have more symmetric electron charge clouds between Li and P atoms than the Na–P and Mg–P bonds. Additionally, the charge density difference around the P atoms is positive (charge accumulation), while it is negative around the Na and Mg atoms (charge depletion). In other words, the Na–P and Mg–P bonds in black phosphorus show more ionic bonding character than Li–P bonds.

To clarify the lithiation, sodiation, and magnesiation mechanisms of black phosphorous, we additionally performed atomic charge analysis for the M_xP (M = Li, Na, and Mg) structures. Fig. 4 shows the distribution histograms of the Bader atomic charge populations of M in M_xP (M = Li, Na, and Mg). Up to the $M_{0.25}P$ composition for all three metals (*i.e.*, showing intercalation mechanisms), their atomic charges have constant values: +0.84*e* for Li, +0.78*e* for Na, and +1.51*e* for Mg. However, after reaching this composition, the charge states of Li, Na, and Mg decrease rapidly and have atomic charge values over wide ranges due to the formation of amorphous M_xP structures from the P–P bond breaking induced by lithiation, sodiation, and magnesiation.

In particular, the atomic charges of Li atoms in $Li_{4.5}P$ range from +0.82*e* to −1.54*e*, those of Na atoms in Na_4P range from +0.77*e* to −0.84*e*, and those of Mg atoms in Mg_2P range from +1.51*e* to −0.12*e*. Here, it is very interesting that some Li, Na, and Mg atoms can have negative atomic charge states at the high Li, Na, and Mg concentrations of $Li_{4.5}P$, Na_4P, and Mg_2P. The emergence of the negative atomic charges results from local clustering of the metal atoms. As shown in Fig. 4, some of the M metal atoms are surrounded by other M atoms at high concentrations, which can prevent interactions between M and P atoms, so that the central M atoms no longer lose electrons to P. For clear understanding, we analyzed the coordination numbers (CNs) of Li, Na, and Mg at high concentrations. From the RDF analysis in Fig. S1 (ESI†), $Li_{4.5}P$ has an average CN_{Li-Li} = 5.65 and CN_{Li-P} = 4.32; however, in some cases, the partial CNs of Li CN_{Li-Li} = 7 and CN_{Li-P} = 1. In the local structures, the CNs deviate from the average values, and the central Li atoms can have a negative atomic charge state (−1.47*e*). We also find partial CNs of Li (CN_{Li-Li} = 5 and CN_{Li-P} = 3) that deviate from the average value; however, in this case, the central Li atom shows a positive charge state (+0.82*e*). Thus, a Li atom that has little interaction with P can have a negative charge state. A similar phenomenon is found in Na_4P and Mg_2P. For instance, we find some Na atoms surrounded by 9 Na atoms in the Na_4P structure. The partial CNs of Na (CN_{Na-Na} = 9 and CN_{Na-P} = 0) in

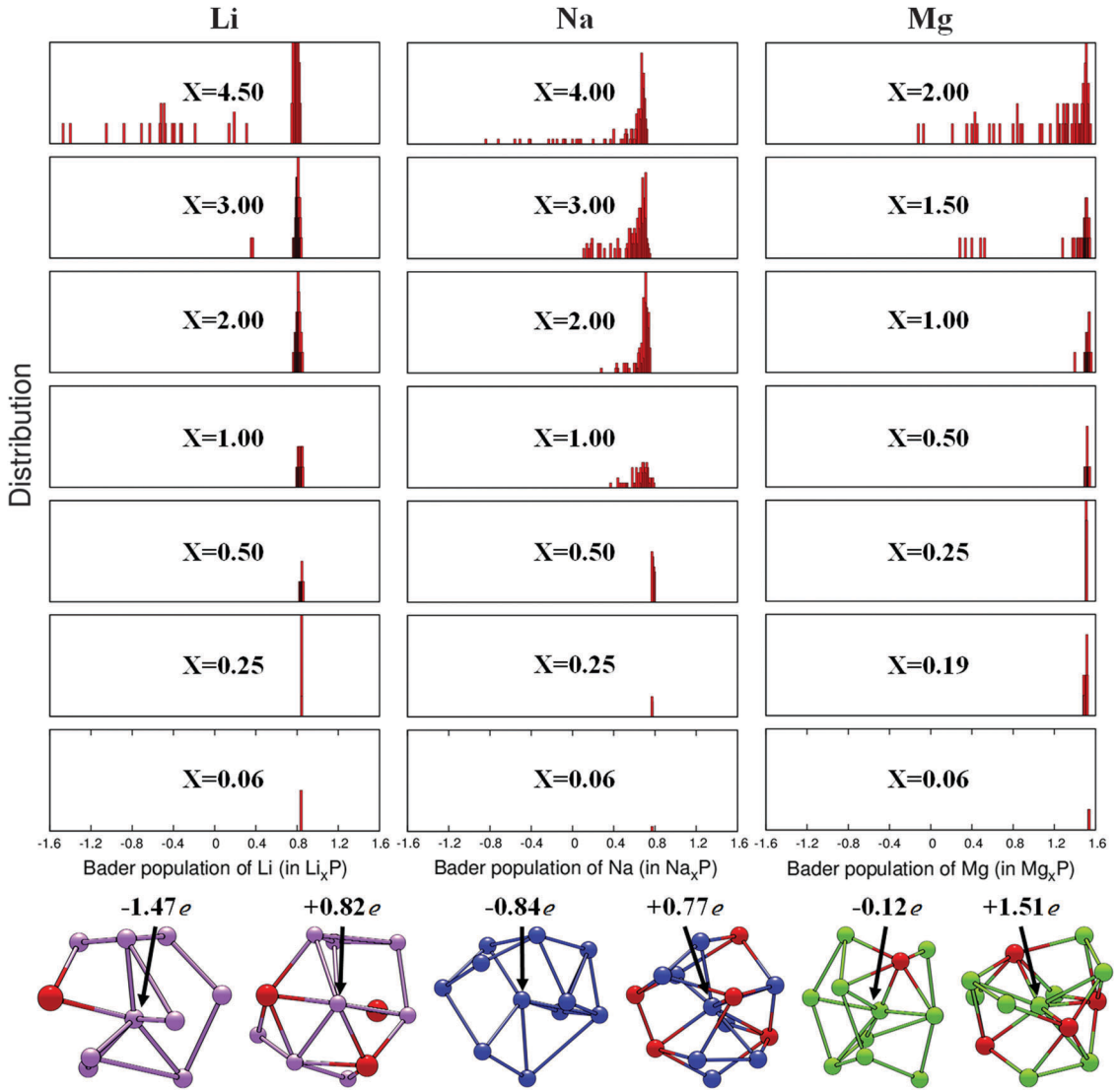

Fig. 4 Distribution histograms of the Bader populations of M in M_xP (M = Li, Na, and Mg). Representative local structures of $Li_{4.5}P$, $Na_{4.0}P$ and $Mg_{2.0}P$ are also shown. Here, the red, pink, navy blue and green atoms represent P, Li, Na, and Mg, respectively.

the local structure considerably deviate from the average values of CN_{Na-Na} = 5.71 and CN_{Na-P} = 4.77. In this case, the Na atom has a negative charge ($-0.84e$).

In addition, the clustering between M metals (M = Li, Na, and Mg) occurs below their maximum metal capacities (*i.e.* $Li_{4.5}P$, $Na_{4.0}P$, and $Mg_{2.0}P$). Indeed, in Fig. 1, we can see that clustering is also found in $Li_{3.0}P$, $Na_{3.0}P$, and $Mg_{1.5}P$, which are lower compositions than the maximum capacities. The trend of the clustering behavior is Li > Mg > Na. It follows their cohesive energies: 1.61 eV (Li) > 1.51 eV (Mg) > 1.11 eV (Na), which is an opposite trend of the ionic size: 0.95 Å (Na^+) > 0.65 Å (Mg^{2+}) > 0.60 Å (Li^+).

3.3. Comparison of the mechanical properties of M_xP (M = Li, Na, and Mg)

Volume expansion behaviors during lithiation, sodiation, and magnesiation are a very important factor that must be considered in the development of an anode material. Usually, a large volume change in an anode material upon lithiation, sodiation, and magnesiation would lead to loss of electrical contact and then rapid capacity fading. Because such volume expansion behaviors are closely related to the mechanical properties of materials, we also studied the properties of M_xP (M = Li, Na, and Mg) in this work.

As previously mentioned, black phosphorus has a corrugated structure, with two different P–P bonds: planar P–P and staggered P–P. In $Li_{0.25}P$ and $Mg_{0.25}P$, as shown in Fig. 5, lithiation and magnesiation lead to preferential breaking of the staggered P–P bonds rather than the planar bonds. Similar behavior is also found in sodiation, although it is observed at a higher concentration ($Na_{0.28}P$ compared with $(Li/Mg)_{0.25}P$). This implies that staggered P–P bonds are weaker than planar bonds. Moreover, we find that P–P bond breaking occurs in $Li_{0.25}P$ and $Mg_{0.25}P$ but not in $Na_{0.25}P$, which implies that the P–P bonds in Na_xP are stronger than those in Li_xP and Mg_xP.

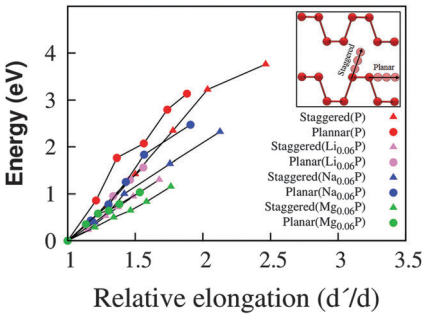

Fig. 5 Energy profile with relative elongation (d'/d) of planar (circle) and staggered (triangle) P–P bonds in pristine black phosphorus (P) and $M_{0.06}P$ (M = Li, Na, Mg), where d is the optimized P–P bond distance and d' is the elongated bond distance. Color codes of pristine P, $Li_{0.06}P$, $Na_{0.06}P$, and $Mg_{0.06}P$ are red, pink, blue, and green, respectively.

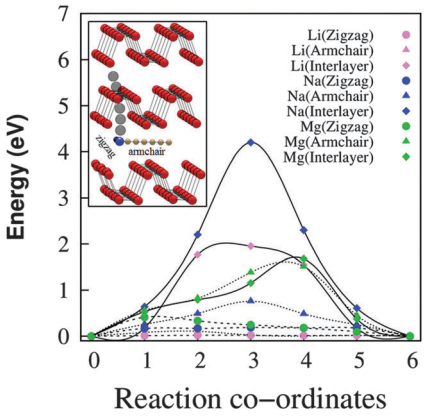

Fig. 6 Diffusion barriers of Li, Na and Mg in black phosphorus along three different diffusion paths. Color codes are pink = Li, blue = Na, and green = Mg.

To compare the P–P bonds in M_xP (M = Li, Na, and Mg), we calculated the energy profile as a function of the P–P bond elongation in $M_{0.06}P$, which is shown in Fig. 5. When calculating the energy change, we optimized the $M_{0.06}P$ structures and performed a cell optimization in which the positions of the two P–P bond atoms were fixed at a given bond distance, while the other P and M atoms were allowed to relax. For $Li_{0.06}P$, $Na_{0.06}P$, and $Mg_{0.06}P$, the planar P–P bonds show steeper slopes than the staggered ones, indicating that more energy is required to break the planar P–P bonds than the staggered ones. Moreover, Li, Na, and Mg intercalations lead to decrease of the slope compared with the black phosphorus case. In other words, the P–P bonds in M_xP are weaker than those in pristine black phosphorus. In particular, the staggered P–P bonds in $Na_{0.06}P$ are the strongest among the staggered P–P bonds in $Li_{0.06}P$, $Na_{0.06}P$, and $Mg_{0.06}P$. This is because the interaction between Na and P atoms is lower than the Li and Mg cases. Thus, the P–P bond character in $Na_{0.06}P$ is closer to that in pristine black phosphorus than those in $Li_{0.06}P$ and $Mg_{0.06}P$. As shown in PDOS of Fig. 3, the contributions of the Na 3s orbitals at the Fermi level are less compared to that of the P 3p orbitals than Li and Mg cases.

To compare the mechanical properties of M_xP systems (M = Li, Na, and Mg), we calculated their bulk moduli (Fig. S3, ESI†) at a constant concentration of M_2P using a DFT method, where the concentration of M_2P was used because the maximum magnesiation concentration is Mg_2P, which is lower than the maximum lithiation and sodiation values ($Li_{4.5}P$ and Na_4P), as shown in Fig. 1. Our DFT calculation for pristine black phosphorus provides a bulk modulus of 46 GPa, which is similar to the reported value of 44 GPa.[34] The lithiation and sodiation lead to softening of the black phosphorus by reducing the bulk modulus from 46 GPa for pristine black phosphorus to 26 GPa for Li_2P and 24 GPa for Na_2P. In contrast, Mg_2P has a bulk modulus of 53 GPa, which is higher than that of pristine black phosphorus. In the M_2P systems, a metal atom is surrounded by several metal atoms, as shown in Fig. 4. Accordingly, the softening and hardening of Li_2P, Na_2P, and Mg_2P basically depend on the mechanical properties of the pristine Li, Na, and Mg in their bulk forms. The softening of Li_2P and Na_2P is attributed to the low bulk moduli of pristine Li (11 GPa) and Na (6 GPa), while the hardening of Mg_2P results from the relatively high bulk modulus of Mg (45 GPa).

3.4. Diffusion of Li, Na, and Mg in black phosphorus

Not only the thermodynamic properties, but also the kinetic behaviors of Li, Na, and Mg in black phosphorus determine the battery properties. Investigating the diffusion behaviors of Li, Na, and Mg atoms in black phosphorus is very important. Thus, we performed nudged elastic band (NEB)[35] calculations for the diffusion of single Li, Na and Mg atoms in black phosphorus (Fig. 6). Here, three possible diffusion paths were considered, of which two correspond to movements along the phosphorene layer and the other corresponds to interpenetration through a phosphorus hexagon ring of a phosphorene layer. For the diffusion behaviors along the phosphorene layer, the Li, Na, or Mg atom hops along the same 1D channel (zigzag direction) or hops to an adjacent channel (armchair direction) along the corrugated path. Interestingly, the diffusion barriers for Li, Na and Mg along the zigzag direction are as low as 0.02 eV for Li, 0.18 eV for Na, and 0.41 eV for Mg, which are lower than those in the armchair direction: 0.12 eV for Li, 0.76 eV for Na and 1.50 eV for Mg. In addition, we find that the energy barriers for interlayer movement are very high compared to the zigzag and armchair diffusions, indicating the difficulty of such diffusion behaviors.

Moreover, the zigzag and armchair Li diffusion barriers in black phosphorus are lower than that of Li diffusion (0.5 eV) in graphite,[36] indicating easier Li diffusion in black phosphorus. This appears to be because the interlayer distance of black phosphorus is longer than that of graphite: 5.4 Å (black phosphorus) *versus* 3.4 Å (graphite).

4. Summary and conclusion

First-principles calculations show that black phosphorous can be used as an electrode material for Li-, Na- and Mg-ion batteries, as it can store Li/Na/Mg atoms up to $Li_{4.5}P$, Na_4P, and Mg_2P. Here, we also clarify the lithiation, sodiation and

magnesiation mechanisms of black phosphorus. The three mechanisms are similar in that an intercalation mechanism (no P–P bond breaking) occurs at low Li/Na/Mg concentrations but changes to an alloying process with P–P bond breaking; Li and Mg show a columnar intercalation mechanism, as they prefer to localize in different phosphorene layers, while Na shows a planar intercalation mechanism, as it prefers to localize in the same layer. The proposed lithiation, sodiation, and magnesiation mechanisms are supported by Bader charge analysis, showing that during the intercalation process, the Li/Na/Mg atoms have constant atomic charges irrespective of the Li/Na/Mg concentration; however, during the alloying process, the atomic charges vary over wide ranges. At high concentrations (*e.g.*, $Li_{4.5}P$, Na_4P, and Mg_2P), some Li/Na/Mg atoms are even observed to have negative atomic charge states, when they are surrounded by many other metal atoms above the average coordination numbers.

The mechanical properties of black phosphorus during lithiation, sodiation, and magnesiation are also studied. During Li/Na insertion at high concentrations (Li_2P and Na_2P), the lithiation and sodiation lead to softening of the black phosphorous (decrease of the bulk modulus); in contrast, the magnesiation process shows a hardening phenomenon (increase of the bulk modulus). The diffusion of Li/Na/Mg in black phosphorus during the intercalation is an easy process. The diffusion of Li even has a lower energy barrier in black phosphorus than in graphite. From these results, we can reach the conclusion that black phosphorus is a promising candidate for use in Li-, Na-, and Mg-ion batteries.

Acknowledgements

We acknowledge the financial support of the Korea Institute of Science and Technology (Grant No. 2E26130 & 2E26330) and the Industrial Strategic Technology Development Program (Grant No. 10041589) funded by the Ministry of Trade, Industry, and Energy (MOTIE) of Korea.

References

1 M. D. Slater, D. Kim, E. Lee and C. S. Johnson, *Adv. Funct. Mater.*, 2013, **23**, 947–958.
2 S. Y. Hong, Y. Kim, Y. Park, A. Choi, N.-S. Choi and K. T. Lee, *Energy Environ. Sci.*, 2013, **6**, 2067–2081.
3 D. Guerard and A. Herold, *Carbon*, 1975, **13**, 337–345.
4 K. Persson, V. A. Sethuraman, L. J. Hardwick, Y. Hinuma, Y. S. Meng, A. van der Ven, V. Srinivasan, R. Kostecki and G. Ceder, *J. Phys. Chem. Lett.*, 2010, **1**, 1176–1180.
5 M. Kawaguchi and A. Kurasaki, *Chem. Commun.*, 2012, **48**, 6897–6899.
6 P. W. Bridgman, *J. Am. Chem. Soc.*, 1914, **36**, 1344–1363.
7 R. Hultgren, N. S. Gingrich and B. E. Warren, *J. Chem. Phys.*, 1935, **3**, 351–355.
8 G. E. Bacon, *Acta Crystallogr.*, 1951, **4**, 558–561.
9 C. M. Park and H. J. Sohn, *Adv. Mater.*, 2007, **19**, 2465–2468.
10 M. Nagao, A. Hayashi and M. Tatsumisago, *J. Power Sources*, 2011, **196**, 6902–6905.
11 C. Marino, A. Debenedetti, B. Fraisse, F. Favier and L. Monconduit, *Electrochem. Commun.*, 2011, **13**, 346–349.
12 L. Q. Sun, M. J. Li, K. Sun, S. H. Yu, R. S. Wang and H. M. Xie, *J. Phys. Chem. C*, 2012, **116**, 14772–14779.
13 J. Qian, D. Qiao, X. Ai, Y. Cao and H. Yang, *Chem. Commun.*, 2012, **48**, 8931–8933.
14 L. Wang, X. He, J. Li, W. Sun, J. Gao, J. Guo and C. Jiang, *Angew. Chem., Int. Ed.*, 2012, **51**, 9034–9037.
15 C. Marino, L. Boulet, P. Gaveau, B. Fraisse and L. Monconduit, *J. Mater. Chem.*, 2012, **22**, 22713–22720.
16 M. C. Stan, J. von Zamory, S. Passerini, T. Nilges and M. Winter, *J. Mater. Chem. A*, 2013, **1**, 5293–5300.
17 J. Sun, G. Zheng, H. W. Lee, N. Liu, H. Wang, H. Yao, W. Yang and Y. Cui, *Nano Lett.*, 2014, **14**, 4573–4580.
18 Y. Kim, Y. Park, A. Choi, N. S. Choi, J. Kim, J. Lee, J. H. Ryu, S. M. Oh and K. T. Lee, *Adv. Mater.*, 2013, **25**, 3045–3049.
19 J. Qian, X. Wu, Y. Cao, X. Ai and H. Yang, *Angew. Chem., Int. Ed.*, 2013, **52**, 4633–4636.
20 J. Song, Z. Yu, M. L. Gordin, S. Hu, R. Yi, D. Tang, T. Walter, M. Regula, D. Choi, X. Li, A. Manivannan and D. Wang, *Nano Lett.*, 2014, **14**, 6329–6335.
21 J. Sun, H.-W. Lee, M. Pasta, H. Yuan, G. Zheng, Y. Sun, Y. Li and Y. Cui, *Nat. Nanotechnol.*, 2015, **10**, 980–985.
22 K. P. S. S. Hembram, H. Jung, B. C. Yeo, S. J. Pai, S. Kim, K.-R. Lee and S. S. Han, *J. Phys. Chem. C*, 2015, **119**, 15041–15046.
23 G. Kresse and J. Furthmüller, *Phys. Rev. B: Condens. Matter Mater. Phys.*, 1996, **54**, 11169–11186.
24 G. Kresse and J. Furthmüller, *Comput. Mater. Sci.*, 1996, **6**, 15–50.
25 J. P. Perdew, K. Burke and M. Ernzerhof, *Phys. Rev. Lett.*, 1996, **77**, 3865–3868.
26 P. E. Blöchl, *Phys. Rev. B: Condens. Matter Mater. Phys.*, 1994, **50**, 17953–17979.
27 S. Grimme, *J. Comput. Chem.*, 2006, **27**, 1787–1799.
28 H. J. Monkhorst and J. D. Pack, *Phys. Rev. B: Solid State*, 1976, **13**, 5188–5192.
29 A. Brown and S. Rundqvist, *Acta Crystallogr.*, 1965, **19**, 684–685.
30 Y. Du, C. Ouyang, S. Shi and M. Lei, *J. Appl. Phys.*, 2010, **107**, 093718.
31 H. Kim, C. Y. Chou, J. G. Ekerdt and G. S. Hwang, *J. Phys. Chem. C*, 2011, **115**, 2514–2521.
32 C. Y. Chou, M. Lee and G. S. Hwang, *J. Phys. Chem. C*, 2015, **119**, 14843–14850.
33 X. Yu, H. Ushiyama and K. Yamashita, *Chem. Lett.*, 2014, **43**, 1940–1942.
34 Q. Wei and X. Peng, *Appl. Phys. Lett.*, 2014, **104**, 251915.
35 G. Henkelman, B. P. Uberuaga and H. Jónsson, *J. Chem. Phys.*, 2000, **113**, 9901–9904.
36 K. Toyoura, Y. Koyama, A. Kuwabara, F. Oba and I. Tanaka, *Phys. Rev. B: Condens. Matter Mater. Phys.*, 2008, **78**, 214303.